Proceedings of IMECE2005
2005 ASME International Mechanical Engineering Congress and Exposition
November 5-11, 2005, Orlando, Florida USA

IMECE2005-79778

STABILITY AND BIFURCATION ANALYSIS OF A FORCED CYLINDER WAKE

N.W. Mureithi
BWC/AECL/NSERC Chair of Fluid-Structure Interaction
Department of Mechanical Engineering
École Polytechnique, Montréal, QC, Canada

M. Rodriguez
BWC/AECL/NSERC Chair of Fluid-Structure Interaction
Department of Mechanical Engineering
École Polytechnique, Montréal, QC, Canada

ABSTRACT

We present a study on the dynamics of a cylinder wake subjected to forced excitation. Williams *et al.* (1992) discovered that the spatial symmetry of the excitation plays a crucial role in determining the resulting wake dynamics. Reflection-symmetric forcing was found to affect the Karman wake much more strongly compared to $Z_2(\kappa,\pi)$ asymmetric forcing. For low forcing amplitudes, the existence of a nonlinear mode interaction mechanism was postulated to explain the observed "beating" phenomenon observed in the wake.

Previous work by the authors (Mureithi *et al.* 2002, 2003) presented general forms of the modal interaction amplitude equations governing the dynamics of the periodically forced wake.

In the present work, numerical CFD computations of the forced cylinder wake are presented. It is shown that the experimentally observed wake bifurcations can be reproduced by numerical simulations with reasonable accuracy. The CFD computations show that the forced wake first looses reflection symmetry followed by a bifurcation associated with vortex merging as the forcing amplitude is increased. A bifurcation analysis of a simplified amplitude equation shows that these two transitions are due to a pitchfork bifurcation and a period-doubling bifurcation of mixed mode solutions.

INTRODUCTION

The Karman wake behind a circular cylinder is a global instability mode manifested following spatio-temporal (absolute) instability over a 'large' region of the cylinder near wake. Two such global modes are possible. The Karman wake corresponds to the so called 'sinuous' mode. A symmetrical 'varicose' mode may also be manifested in the form pairs of vortices symmetrically shed behind the cylinder.

Although the symmetrical varicose mode is intrinsically unstable, it may be stabilized by cylinder motion. Thus interaction between symmetrical shedding and structural motion has been shown to lead to self-excited vibration of the structure (King 1977, Naudascher 1987). The problem of forced cylinder motion in flow has been considered, for instance, by Naudascher (1986), Williamson & Roshko (1988), Ongoren & Rockwell (1988) and Williams *et al.* (1992). Lateral (cross-flow) and inflow forced oscillation of a cylinder was performed over a range of frequencies and amplitudes. In this parameter space, complex sheddings modes synchronized to the cylinder oscillations were discovered. Synchronized patterns (modes) labeled according to the number of vortices shed per cycle of cylinder oscillation, included 2S, 2P, P+S and 2P+2S; S and P indicate single vortex and pairs of vortices, respectively. Wake (spatio-temporal) symmetry was found to depend strongly on natural shedding to forcing frequency ratio. For low amplitude forcing, modes involving coalescence of large numbers of vortices were found. In Williams *et al.*'s experiments apparent period-doubling was found to occur during symmetric forcing for intermediate forcing amplitudes. 'Simple' symmetry rules were proposed to describe the fundamental wake structure differences for symmetric and antisymmetric forcing.

Recent work by Mureithi *et al.* (2002-2004) has quantitatively established the important role that symmetry plays in the dynamics of the forced cylinder wake. In particular

amplitude equations governing the nonlinear dynamics of mode interactions have been derived based on symmetry equivariant theory. The present paper reports recent developments in this ongoing work. While period-doubling was observed in experimental tests reported in Mureithi *et al.* (2002), the complexity of the turbulent flow made it difficult to discern the dynamics underlying the observed transitions in the wake flow. To overcome this difficulty, the cylinder wake flow is simulated numerically eliminating the effects of extraneous experimental noise. Flow turbulence, known to play at best a secondary role in the wake bifurcation dynamics, is ignored.

CFD COMPUTATIONS

Numerical simulations have been performed using the CFD code Fluent. A rectangular domain around a circular cylinder, having diameter *D*, was generated using the Fluent preprocessor Gambit. Computation domain boundaries were set at 15*D* upstream, 40*D* downstream and 20*D* on the lateral sides. Special care was required to avoid the influence of the boundaries. To solve the Navier-Stokes equations, Fluent uses a standard path in finite volume. A second order upwind scheme was used to obtain the face values needed for the integral computations. A second order temporal integration was performed during the simulations. Modelling of the cylinder motion was done using time dependent inertia forces and boundary conditions to simulate the problem in the non-Galilean cylinder reference frame. Time dependent conditions were input to Fluent by defining a UDF (User Defined Function). Simulations were all carried out for a flow at Re=1000. At this Reynolds number the cylinder wake is three dimensional and turbulent. However, as also justified in Blackburn *et al.* (1999), the two dimensional harmonic forcing of the cylinder will produce flows more two dimensional than the fixed cylinder wake. Furthermore the stochastic three-dimensional perturbations associated with flow turbuluence are not believed to be of primary importance *vis-à-vis* the global wake bifurcation dynamics considered in this study. As an example, the primary Hopf bifurcation responsible for the Karman wake shedding is independent of the detailed flow turbulence structure being governed by the form of the velocity profile in the cylinder wake.

Test case

The case of the fixed cylinder was used to validate the numerical model and the accuracy of the simulation results. A series of structured meshes, each time more refined, were tested up to spatial convergence. The final mesh chosen has the following characteristics: 260000 elements (corresponding to 125000 nodes and 135000 cells). Special care was required in meshing the cylinder boundary layer, which is excited by the moving cylinder. The time step was chosen to capture the dynamics of the wake. It was equal to one hundredth of the vortex-shedding period. The accuracy of our results has been verified by comparing our drag and lift coefficient (respectively C_d, C_l) and Strouhal number (St) values to some experimental and numerical data, as shown in Table 1. The computed drag coefficient has a mean value of 1.27. The *rms* lift coefficient is 0.85, while the Strouhal number is approximately 0.24.

Re = 1000	St	C_d	C_l
Our results	0.237	1.27	0.85
Hua et al. (2005) *computation*	0.239	1.49±0.2	0.98
Roshko (1954) *experiments*	0.21	1.2	-

Table 1. Summary of present results compared to other computational and experimental data.

The Strouhal number is high compared to experimental results but the value is reasonable when compared to other two dimensional CFD simulations. The drag coefficient is larger than that found experimentally by Roshko (1954). This can be explained by the absence of turbulence modelling in our simulations as justified earlier. The lift coefficient results are close to those of Hua *et al. (*2005).

Figure 1 shows the Von Karman wake downstream of the cylinder. The change in the wake structure beyond ten diameters downstream is in agreement with experimental observations (see Van dyke (1982)) and the computation results of Hua *et al.* (2005).

The foregoing verification is for the fixed cylinder case. The validation of the moving cylinder simulations may be found in the results and discussion sections of the paper.

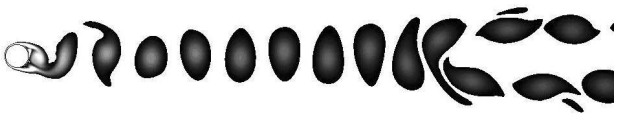

Figure 1. Vorticity field (s^{-1}) past a fixed cylinder

Simulation results

Simulation results are presented for the case of a cylinder oscillating harmonically in the stream-wise direction at a frequency *f* equal to the Karman vortex shedding frequency f_v behind the fixed cylinder, thus $f/f_v=1$. The cylinder oscillation amplitude (*A*) was varied from the stationary cylinder case (A/D=0) to a ratio A/D=0.4. Moving cylinder simulations were initiated starting from the stationary cylinder Karman shedding solution. Simulations were carried out to attain a steady-state in the cylinder's wake and then simulated during 50 periods of the cylinder's oscillation (T_e).

Vortex dynamics analysis

We now proceed to describe the changes in vortex wake modes as a function of cylinder oscillation amplitude. Looking at the wake flow in terms of the vortex wake mode behind the cylinder the strong effect of the cylinder motion is apparent. For small amplitudes, as shown for A/D=0.05 in Figure 2, the vortex shedding locks into the cylinder motion, with two single vortices shed per cycle of cylinder oscillation. Compared to the fixed cylinder case, the vortex shedding process is similar but vortex evolution downstream the cylinder is slightly perturbed.

Figure 2. Vorticity field (s^{-1}) past an oscillating cylinder in the stream wise direction, A/D=0.05.

For *A/D*=0.2, reflection-symmetry breaking occurs in the vortex wake dynamics, as seen in Figure 3. Referring to Williamson and Roshko's (1988) wake mode definitions, the present wake mode is identified as being a P+S mode. Forced oscillations have broken the wake reflection symmetry. During every period of cylinder oscillation a single vortex and a pair of vortices are shed from the cylinder. Further downstream the pair of opposite vortices separates while the single vortex shed half a period later is attracted by the separated vortex of opposite sense giving the resulting P+S mode (Pair + Single vortex shed per cycle of cylinder motion).

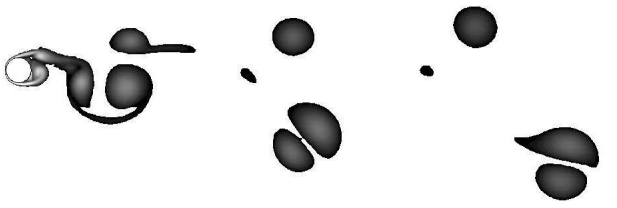

Figure 3. Vorticity field (s^{-1}) past an oscillating cylinder in the streamwise direction, A/D=0.2.

From the simulation results, the flow can destabilize by symmetry breaking in two ways without preference (Figures 3 and 4). This characteristic symmetry breaking of the flow can be compared to the buckling of a beam subjected to an increasing axial load. In both cases a reflection symmetry is broken. The mirror image of the flow, shown in Figure 4, could also have been obtained using a small perturbation of the inflow velocity destabilizing the wake in the other sense for *A/D*=0.2 in Figure 3.

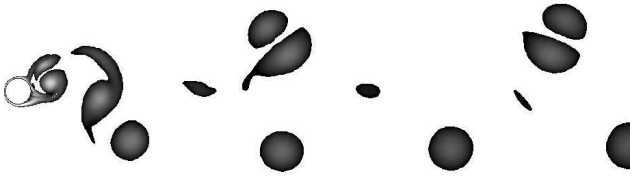

Figure 4. Vorticity field (s^{-1}) past an oscillating cylinder in the streamwise direction, A/D=0.25.

Finally, for higher amplitudes the S mode is clearly identified. The identification 'S' indicates that a single vortex is shed per cycle of cylinder oscillation. This mode results from vortex coalescence just downstream of the cylinder. The pair of opposite vortices and the single vortex shed half a period later merge into a single large vortex, which has the same sense as the single vortex shed from the cylinder a short time later, as shown in figure 5. The effect of larger amplitude cylinder oscillation is therefore to induce a period-doubling in the wake flow. Only one vortex results from every period of oscillation of the flow.

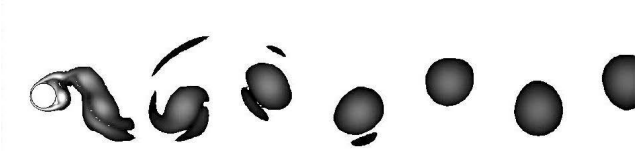

Figure 5. Vorticity field (s^{-1}) past an oscillating cylinder in the streamwise, direction A/D=0.4.

Proper Orthogonal Decomposition

In order to understand the effect of external forcing on the Karman wake, a proper orthogonal decomposition (POD) of the flow has been performed to extract spatio-temporal modes. The fluctuating x-velocity *u'* has been recorded at each time step at 141 points along a line transverse to the flow located ten diameters (10*D*) downstream of the cylinder during $50T_e$. The fluctuating velocity is defined by

$$u'(y,t) = u(y,t) - \langle u(y,t) \rangle .$$

POD is an orthogonal decomposition that gives coherent spatio-temporal structures capturing the maximum of the velocity field energy. Each mode is composed of spatial components $a_k(t)$ referred to as 'topos', and temporal ones $\psi_k(y)$, the 'chronos', such that we can write,

$$u'(y,t) = \sum a_k(t)\psi_k(y) .$$

Decomposing the flow past the stationary cylinder, mainly two modes are found as seen in Figure 6; (note that Figures 6-13 are at the end of the paper). The first mode has an odd (anti-symmetric) topos and a chronos with a principal frequency equal to f_v. The second mode is even (reflection-symmetric) at a frequency $2f_v$. This decomposition confirms that the Karman wake is equivalent to the superposition of a sinuous mode and a varicose mode at twice the vortex shedding frequency. As the square of the singular value corresponding to each mode represents the energy of the mode, the first mode contains close to 99% of the energy of the flow and the second close to 1%. The remaining modes are found to be negligible. The squares of the singular values for the different modes are presented in Figure 7.

For small oscillation amplitudes the POD decomposition, Figure 8, gives an odd first mode at f_v but now a second even mode having frequency f_v as opposed to $2f_v$ for the fixed cylinder case. For small amplitudes of oscillation, the topos does not have a clear harmonic decomposition, unlike the fixed cylinder case. The second mode corresponds to the symmetric forcing which is now significant in terms of energy transferred to the flow (more than 10%), as shown in Figure 9.

From *A/D*=0.2 to *A/D*=0.35, POD does not give distinguished modes in terms of odd-even symmetry.

Furthermore the chronos components lack single well defined frequencies. This suggests a transition range of amplitudes. Figures 10 and 11 show, respectively, the first two modes in terms of topos and chronos. The graphs presenting the squares of the corresponding singular values confirm the absence of a principal and well defined mode.

For superior *A/D* values, POD decomposition gives a first mode, which is odd, having a frequency $f_v/2$ and a second, even, mode at f_v. Now the topos shapes are the same as in the fixed cylinder case as seen figure 12. The graph of the values, Figure 13, shows that most of the energy is contained in the first odd mode compared to the second one whose characteristics in terms of symmetry and frequency correspond to the forcing of the flow. This signifies an energy transfer from the second mode to the first.

POD and vortex wake modes comparison

Numerical simulations of the flow and POD analysis give insight into the wake dynamics which can be summed up as follows. After a lock-in state of the vortex wake for small oscillation amplitudes where the 2S vortex wake is composed of an odd mode at the vortex shedding frequency and an even mode resulting from the forcing, the flow bifurcates by (reflection) symmetry breaking. The resulting wake has a P+S vortex mode and is not composed of distinct symmetric and quasi-harmonic modes. Still increasing the cylinder amplitude, the flow bifurcates next via period-doubling. For *A/D* above 0.35 the POD decomposition gives topos of the same shape as that found in the fixed cylinder case but now coupled with chronos evolving at half the shedding frequency. A complete period-doubling has now occurred.

WAKE FLOW SYMMETRY AND AMPLITUDE EQUATIONS

The procedure for the derivation of the mode amplitude equations is briefly described in this section. This is followed by a qualitative bifurcation analysis and comparison with the CFD simulation results. The amplitude equations have been derived using equivariant ('symmetry') bifurcation theory. For details, the reader is referred to Mureithi *et al.* (2002, 2003).

Starting slightly downstream of the cylinder the base flow symmetry is $\Gamma = Z_2(\kappa)\times SO(2) = O(2)$. The reflection symmetry $Z_2(\kappa)$ is defined relative to a line through the cylinder center and parallel to the upstream flow. With $u(x,y,t)$ being the local inflow velocity the 2D flow symmetry above means the following relations hold:

$$\begin{aligned} u(x,y,t) &= u(x+l,y,t) \\ u(x,y,t) &= u(x,-y,t) \end{aligned} . \tag{1}$$

Equivalent relations exist for the transverse velocity component.

To study the dynamics of modal interaction between the Karman wake shedding mode (**K**) and the reflection symmetric mode **S** we assume that all other flow modes are stable. In this case all flow perturbations (pressure, velocity etc.) may be expressed as the sum of the mode **S** and mode **K** component fields. As an example, the *x*-direction velocity perturbation takes the form

$$\begin{aligned} u(x,y,t) = S(t)\psi_S(y)e^{i(\lambda_S x+\omega_S t)} \\ + K(t)\psi_K(y)e^{i(\lambda_K x+\omega_K t)} + c.c. \end{aligned} \tag{2}$$

$S(t)$ and $K(t)$ being the mode amplitudes for mode **S** and **K**, respectively. The respective mode **S** and mode **K** symmetries are

$$\begin{aligned} \Gamma_S &= D_m(\kappa,\frac{2\pi}{m})\times S^1 \\ \Gamma_K &= Z_2(\kappa,\pi)\times S^1 \end{aligned} \tag{5}$$

where '*m*' is the wavelength ratio λ_K/λ_S. Γ_S and Γ_K are subgroups of the base symmetry Γ. Based on these inherent symmetry properties the mode **S** *x*-velocity field satisfies the relations

$$\begin{aligned} u(x,y,t) &= u(x,-y,t) \\ &= u(x+\lambda_S,y,t) = u(x,y,t+\tau_S) \end{aligned} . \tag{3}$$

The **K** mode x-velocity satisfies the relation

$$\begin{aligned} u(x,y,t) &= u(x,-y,t+\tau_K/2) \\ &= u(x+\lambda_K/2,-y,t) \end{aligned} . \tag{4}$$

Note that λ and τ are the wavelength and period respectively.

We seek the amplitude interaction equations in the discrete form

$$X_{n+1} = \Phi(X_n) \tag{6}$$

where $X_n = [S_n \;\; K_n]^T$ and discretization is with respect to the vortex shedding period. The symmetry group Γ constrains the form of the function $\Phi(X_n)$. For each symmetry element $\gamma\in\Gamma$, the following relation must hold:

$$\gamma\Phi(X_n) = \Phi(\gamma X_n), \qquad \forall\gamma\in\Gamma,\ \forall X\in C^2. \tag{7}$$

The Γ-equivariance constraint (7) of $\Phi(X_n)$ has been used to derive the most general form of the equation governing the interaction between the **S** and **K** modes which is presented in the following lemma:

Lemma (Mureithi et al., 2002) *Every* $\Gamma = Z_2(\kappa)\times SO(2)$ *equivariant map* $\Phi: C^2\to C^2$ *has the form*

$$\Phi(S,K) = \begin{bmatrix} p(r_1,r_2,r_3)S + q(r_1,r_2,r_3)\overline{S}^{n-1}K^m \\ r(r_1,r_2,r_3)K + s(r_1,r_2,r_3)S^n,\overline{K}^{m-1} \end{bmatrix}$$

for m=2k, and

$$\Phi(S,K)=\begin{bmatrix} p(r_1,r_2,r_4)S+q(r_1,r_2,r_4)\overline{S}^{2n-1}K^{2m} \\ r(r_1,r_2,r_4)K+s(r_1,r_2,r_4)S^{2n}\overline{K}^{2m-1}\end{bmatrix}$$

for $m=2k-1.$

where p,q,r,s *are real polynomial functions of the* $\Gamma-$*invariants* $r_1=|S|^2$, $r_2=|K|^2$ $r_3=S^n\overline{K}^m$ *and* $\overline{r}_3$.

For $\lambda_K/\lambda_S=m/n=1$ the amplitude equations in polar form with

$$K=re^{i\phi},\ S=qe^{i\psi} \tag{8}$$

are

$$\begin{aligned} r_{n+1}&=\left(1+\alpha_0+\alpha_2r_n^2+\gamma_{11}q_n^2\right)r_n+\delta_{01}q_n^2r_n\cos 2\theta_n \\ q_{n+1}&=\left(1+\beta_0+\beta_2q_n^2+\gamma_{21}r_n^2\right)q_n+\mu_{01}q_nr_n^2\cos 2\theta_n \\ \theta_{n+1}&=\theta_n-q_nr_n(\mu_{01}r_n+\delta_{01}q_n)\sin 2\theta_n \end{aligned} \tag{9}$$

where $\theta_n=\psi_n-\phi_n$. Steady state solutions are obtained for $\cos 2\theta=\pm 1$. These solutions are mixed mode solutions containing a 'mixture' of the **S** and **K** modes. The solution symmetry is a common subgroup of Γ_S and Γ_K.

To determine the interaction dynamics implied by the mapping (8), the symmetrical mode **S** may be treated as a known 'parameter' that can be varied as done in both the physical and the numerical experiments; (clearly this is only an approximation since forced cylinder motion does not generate (or excite) the uniform S-mode throughout the flow field). The assumption, however, makes it possible to reduce the mapping (8) to a single equation for the modal amplitude K. Mureithi *et al.* (2002) showed that the solution of the resulting mapping depends on the quantity $\gamma_{11}-\delta_{01}$. They also showed, based on test data, that $\gamma_{11}-\delta_{01}>0$. This leads to two possible solutions $\overline{r}_1$ and $\overline{r}_2$ for the (now) mixed-mode amplitude *r*. The two solution depend on whether we suppose $\cos 2\theta=+1$ or $\cos 2\theta=-1$. Depending on the solution, both a pitchfork bifurcation and a period-doubling bifurcation are predicted.

The condition $\gamma_{11}-\delta_{01}>0$ leads to two possibilities, (a) $\gamma_{11}>\delta_{01}>0$, (b) $\gamma_{11}<\delta_{01}<0$.

Case (a) $\gamma_{11}>\delta_{01}\geq 0$

In this case the stability derivative $f_{,r}(\overline{r}_i),\ i=1,2$ approaches -1 for large forcing amplitude S. The two solutions $\overline{r}_1$ and $\overline{r}_2$ exist for all values of forcing amplitude S. The solution $\overline{r}_2$ grows faster, but destabilizes faster as well.

Case (b) $\gamma_{11}<\delta_{01}\leq 0$

In this second case, while the solution $\overline{r}_1$ exists for all forcing amplitudes, the solution $\overline{r}_2$ exists only in the range $0<S^2\leq\dfrac{-\gamma_{11}}{\gamma_{11}+\delta_{01}}$. This solution disappears in a pitchfork bifurcation since as S increases the stability derivative $f_{,r}(\overline{r}_2)\to+1$. The $\overline{r}_2$ solution grows faster (with S) but also destabilizes faster than the $\overline{r}_1$ solution as the forcing amplitude S increases. The slower growing $\overline{r}_1$ solution later (at higher S) destabilizes via a period doubling bifurcation as the stability derivative $f_{,r}(\overline{r}_1)\to-1$.

Based on the foregoing, the following bifurcation scenario is proposed as a possible explanation of the CFD simulation results reported earlier. When the cylinder forcing S is introduced two mixed mode solutions (containing S and K 'components') appear. This explains the mixture of symmetrical and asymmetrical components in the POD decompositions for low forcing amplitudes near A/D=0.2 (Figure 12). The amplitudes of these solutions are respectively, $\overline{r}_1$ and $\overline{r}_2$. The two solutions have different stability properties. The solution $\overline{r}_2$ has a higher growth rate. This solution also destabilizes at lower values of forcing S. We conjecture that it is the pitchfork-bifurcation-induced instability of this solution that leads to the observed P+S flow mode (or wake pattern) obtained in the numerical simulations starting near *A/D*=0.2 (see Figures 3 and 4).

The solution $\overline{r}_1$ continues to grow as the forcing amplitude increases ultimately suffering a period-doubling bifurcation. This leads to the manifestation of the S-mode observed in the CFD computations and previously in experiments by Mureithi *et al.* (2002). The pitchfork and period-doubling bifurcations could have been easily deduced from symmetry considerations. The pitchfork bifurcation is associated with a breaking of the $Z_2(\kappa)$ reflection symmetry component while the period-doubling bifurcation results from a maximal breaking of the π-translation symmetry (where π corresponds to a half-period translation in space).

CONCLUDING REMARKS

The cylinder wake has been found to undergo a series of bifurcations when forced oscillations are introduced in the flow direction. Preliminary results indicate that a symmetry based analysis is able to capture and explain the observed wake transitions as the forcing amplitude is increased. In particular reflection-symmetry breaking leads to the visually asymmetrical P+S flow mode. This mode appears as a result of the pitchfork bifurcation of a mixed-mode flow state. This mixed-mode state was well highlighted by the POD analysis which revealed the non-dominance of pure symmetrical or asymmetrical modes for low forcing amplitudes prior to the pitchfork bifurcation. When the forcing amplitude is high enough, a period-doubling instability of the second mixed-mode solution is predicted. The S flow mode solution is a manifestation of the period-doubling instability.

REFERENCES

Blackburn, H.M., and R.D. Henderson: "A study of two-dimensional flow past an oscillating cylinder", *J. Fluid Mech.,* 385, 255-286 (1999).

Hua, C., R.P. LeBeau , and P.G. Huang, "A Cell-Centered Pressure Based Method for Unstructured Incompressible Navier-Stokes Solvers," *43rd AIAA Aerospace Sciences Meeting and Exhibit, AIAA-2005-0880*, Reno, NV, January 10-13, 2005.

King, R. 1977 A Review of vortex shedding research and its applications, Ocean Engineering, Vol.4, pp.141-171.

Mureithi, N.W., Kanki, H., Goda, S., Nakamura, T., and Kashikura, T., 2002, Symmetry breaking and mode interaction in vortex-structure interaction, Paper IMECE 2002-32512, *Proceedings, 5th International Symposium on FSI, AE & FIV+N, ASME Int'l Mech. Engrg. Congress & Exhibition*, New Orleans, Louisiana, USA.

Mureithi N.W., 2003, Implications of symmetry in inline and Karman shedding mode interaction, *NAGARE Journal of the Japanese Society of Fluid Mechanics,* **22**, 211-227.

Mureithi, N.W. et al., 2004, "Response of the Karman wake to external periodic forcing and implication to vortex shedding control", Proc. *8th International Conference on Flow-Induced Vibrations,* Paris, France, 6-9 July 2004.

Naudascher, E. 1987 Flow-induced stream-wise vibrations of structures. *Journal of Fluids and Structures* **1,** 265-298.

Ongoren, A. and Rockwell, D. 1988 Flow structure from an oscillating cylinder, Part I&II. *Journal of Fluid Mechanics* **191,** 197-223, 225-245.

Roshko, A., "On the Development of Turbulent Wakes from Vortex Sheets," *NACA Report* 1191, 1954.

Van Dyke, M. 1982 An album of fluid motion, *Parabolic Press*.

Williamson C.H.K. and Roshko, A. 1988 Vortex formation in the wake of an oscillating cylinder, *Journal of Fluids and Structures* 1988, **2,** 355-381.

Williams D.R., Mansy H. and Amato C. 1992 The response and symmetry properties of a cylinder wake subjected to localized surface excitation. *Journal of Fluid Mechanics* **234,** 71-96.

Williamson, C.H.K. and A. Roshko: "Vortex formation in the wake of an oscillating cylinder", *Journal of Fluids and Structures*, 2, 355-381 (1988).

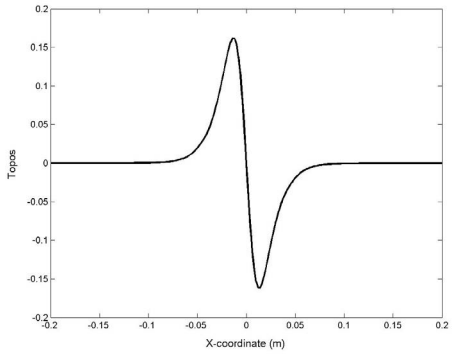

Figure 6a. Fixed cylinder first mode Topos.

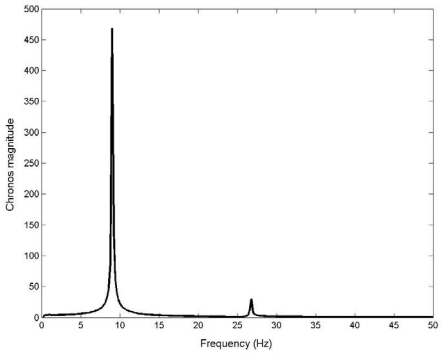

Figure 6b. First mode Chronos for a fixed cylinder.

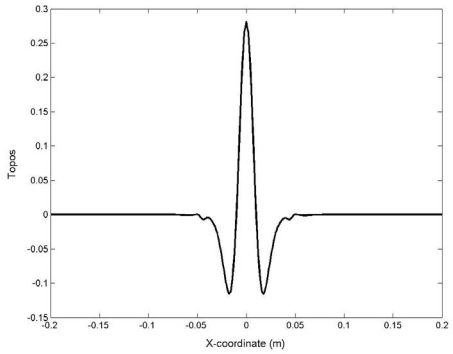

Figure 6c. Second mode Topos for a fixed cylinder.

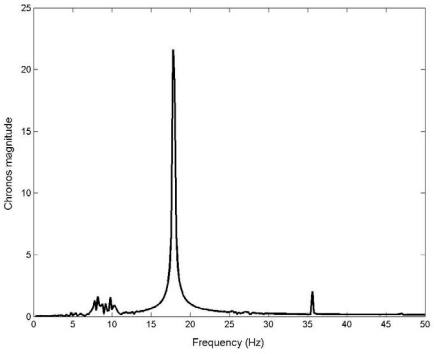

Figure 6d. Second mode Chronos for a fixed cylinder.

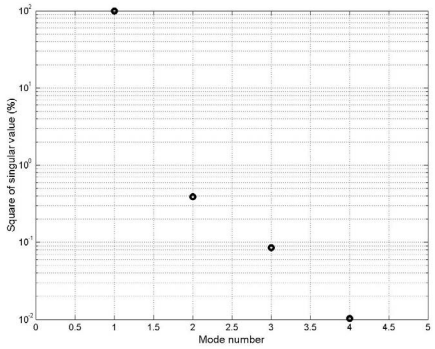

Figure 7. Square of singular value for each mode,(fixed cylinder case).

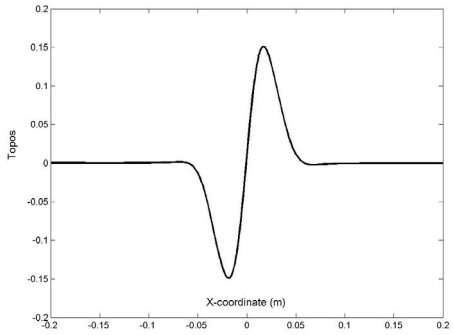

Figure 8a. First mode Topos for A/D=0.05.

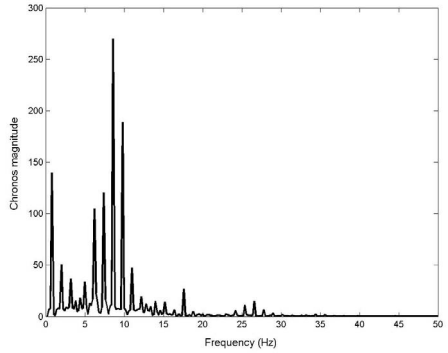

Figure 8b. First mode Chronos for A/D=0.05.

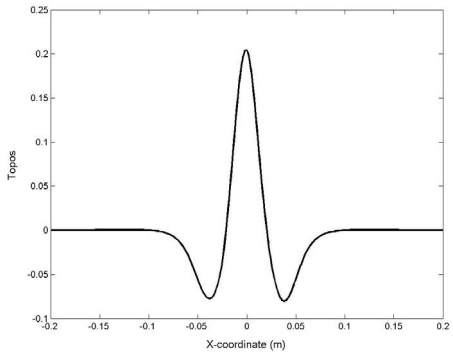

Figure 8c. Second mode Topos for A/D=0.05.

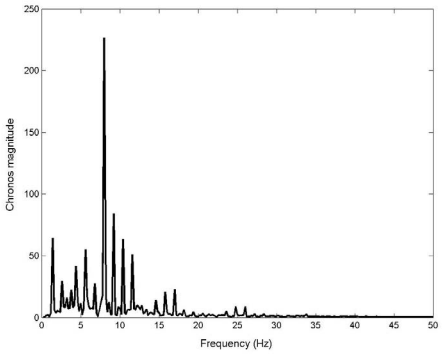

Figure 8d. Second mode Chronos for A/D=0.05.

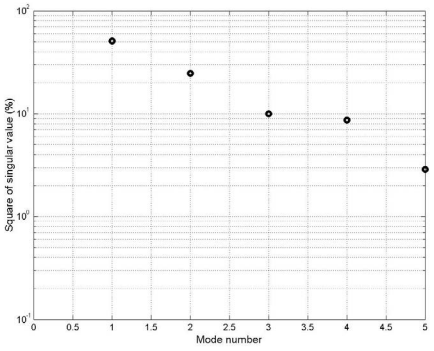

Figure 9. Square of singular values for A/D=0.05.

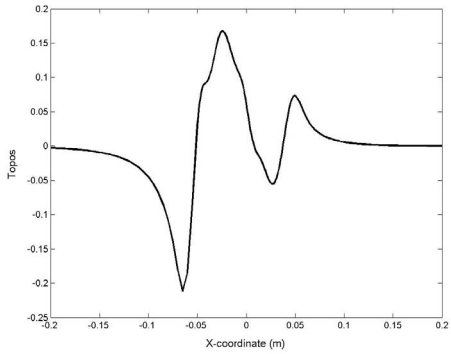

Figure10a. First mode Topos for A/D=0.2.

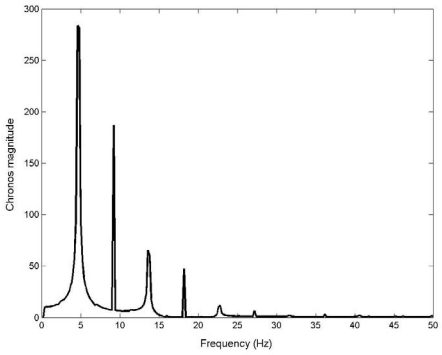

Figure10b. First mode Chronos for A/D=0.2.

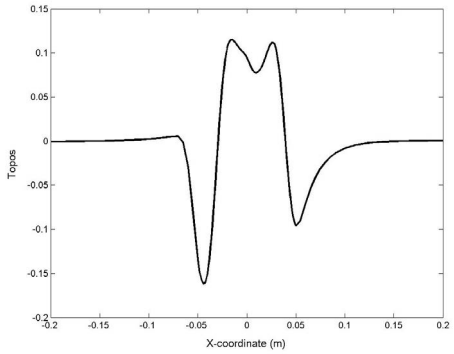

Figure10c. Second mode Topos for A/D=0.2.

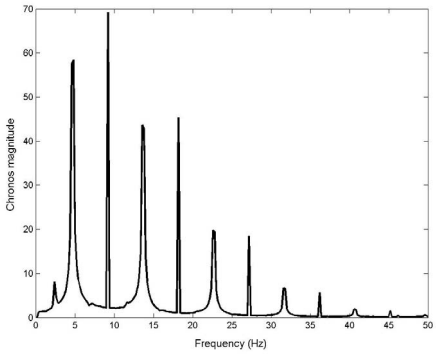

Figure10d. Second mode Chronos for A/D=0.2.

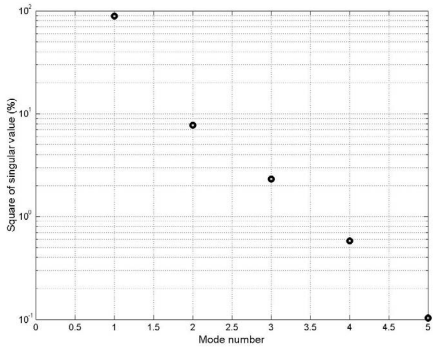

Figure 11. Square of singular values for A/D=0.2.

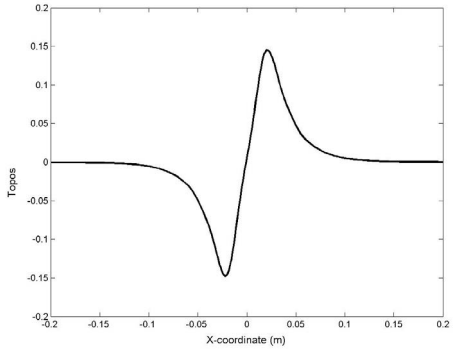

Figure 12a. First mode Topos for A/D=0.4.

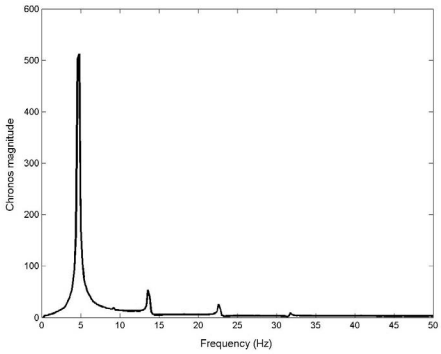

Figure 12b. First mode Chronos for A/D=0.4.

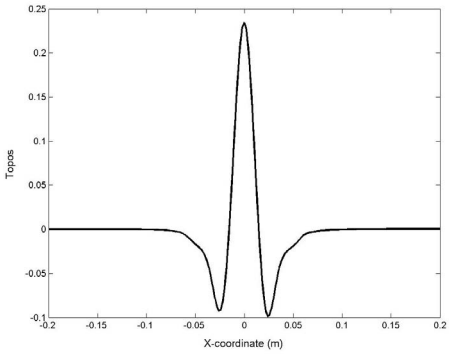

Figure 12c. Second mode Topos for A/D=0.4.

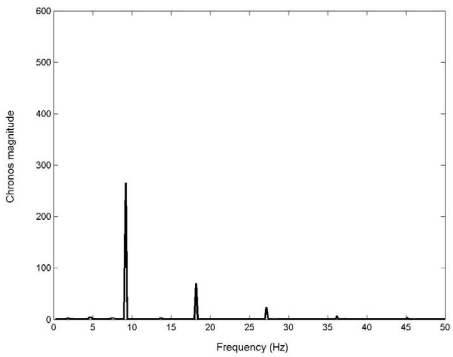

Figure 12d. Second mode Chronos for A/D=0.4.

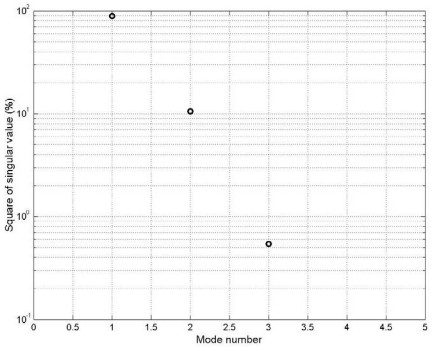

Figure 13 . Square of singular values for A/D=0.4.